Astronomy & Astrophysics manuscript no. KBB22
January 21, 2022

On the Shallowness of Circulation in Hot Jupiters

Advancing the Ohmic Dissipation Model

H. Knierim[1], K. Batygin[2], and B. Bitsch[1]

[1] Max-Planck-Institut für Astronomie, Königstuhl 17, Heidelberg 69117, Germany
[2] Division of Geological and Planetary Sciences California Institute of Technology Pasadena, CA 91125, USA

Received 5 November 2021 / Accepted 19 January 2022

ABSTRACT

The inflated radii of giant short-period extrasolar planets collectively indicate that the interiors of hot Jupiters are heated by some anomalous energy dissipation mechanism. Although a variety of physical processes have been proposed to explain this heating, recent statistical evidence points to the confirmation of explicit predictions of the Ohmic-dissipation theory, elevating this mechanism as the most promising candidate for resolving the radius inflation problem. In this work, we present an analytic model for the dissipation rate and derive a simple scaling law that links the magnitude of energy dissipation to the thickness of the atmospheric weather layer. From this relation, we find that the penetration depth influences the Ohmic dissipation rate by an order of magnitude. We further investigate the weather layer depth of hot Jupiters from the extent of their inflation and show that, depending on the magnetic field strength, hot Jupiter radii can be maintained even if the circulation layer is relatively shallow. Additionally, we explore the evolution of zonal wind velocities with equilibrium temperature by matching our analytic model to statistically expected dissipation rates. From this analysis, we deduce that the wind speed scales approximately like $1/\sqrt{T_{\rm eq} - T_0}$, where T_0 is a constant that evaluates to $T_0 \sim 1000\,{\rm K} - 1800\,{\rm K}$ depending on planet-specific parameters (radius, mass, etc.). This work outlines inter-related constraints on the atmospheric flow and the magnetic field of hot Jupiters and provides a foundation for future work on the Ohmic heating mechanism.

Key words. Magnetohydrodynamics (MHD) – Planets and satellites: atmospheres – Planets and satellites: magnetic fields – Planets and satellites: interiors – Planets and satellites: gaseous planets

1. Introduction

Generic models of giant planetary structures hold that the radii of evolved Jovian-class planets cannot significantly exceed the radius of Jupiter (Stevenson 1982). Accordingly, measurement of the substantially enhanced radius of HD 209458 b – clocking in at $1.39\,R_{♃}$ ($0.73\,M_{♃}$, 1476.81 K, Stassun et al. 2017) – came as a genuine surprise (Charbonneau et al. 2000; Henry et al. 2000). Subsequent detections demonstrated that HD 209458 b is not anomalous; rather, inflated radii are a common attribute of the hot Jupiter (HJ) class of exoplanets (Bodenheimer et al. 2003; Laughlin et al. 2011). This begs the obvious question: what is the physical mechanism that inflates the radii of hot Jupiters?

Although a number of hypotheses have been proposed – for example: tidal heating (e.g., Bodenheimer et al. 2001), thermal tides (e.g., Arras & Socrates 2010), advection of potential temperature (e.g., Tremblin et al. 2017), or the mechanical greenhouse effect (e.g., Youdin & Mitchell 2010) – recent data indicates that explicit predictions of the Ohmic dissipation (OD) mechanism (e.g., Batygin & Stevenson 2010; Wu & Lithwick 2012; Spiegel & Burrows 2013; Ginzburg & Sari 2016) are consistent with the modern dataset. Specifically, the functional form of the inflation profile, and its (Gaussian) dependence on the planetary equilibrium temperature, is reflected in the data (Thorngren & Fortney 2018; Sarkis et al. 2021).[1] In light of this, in this work, we aim to advance the theoretical understanding of the OD mechanism and pose a simple question: how does Ohmic heating depend on the depth to which large-scale atmospheric circulation penetrates? Additionally, we examine if the empirical inflation profile derived from the data itself can constrain the shallowness of circulation layers on these highly irradiated planets.

General circulation models based on "primitive" equations of hydrodynamics routinely find winds in the km s^{-1} range that penetrate to depths on the order of 1 to 10 bars (e.g. Showman et al. 2015; Rauscher & Menou 2013). Menou (2020), however, argues that this depth can actually be significantly greater. Analytic models based on force-balance considerations (Menou 2012; Ginzburg & Sari 2016) or regarding the HJ atmosphere as a heat engine (Koll & Komacek 2018) have predicted similarly fast winds, with magnetic drag dominating at high equilibrium temperatures. On the contrary, anelastic magnetohydrodynamic (MHD) simulations find rather shallow circulation layers with slow wind velocities in general (e.g., Rogers & Komacek 2014; Rogers & Showman 2014; Rogers 2017).

Given that each of these models is subject to their own strengths and limitations, an alternative constraint on HJ circulation patterns is desirable. Accordingly, by extending the Ohmic heating model to include varying zonal wind geometries, we demonstrate the existence of a simple scaling law that allows us to predict the wind depth of HJs from the extent of their inflation under the assumption that Ohmic heating constitutes the dominant interior energy dissipation mechanism.

Another point of considerable interest is the evolution of wind patterns with equilibrium temperature. Force balance arguments suggest strong magnetic damping of equatorial winds

[1] The other inflation models scale like power laws, meaning that their efficiency keeps increasing with equilibrium temperature.

at high equilibrium temperatures $T_{\rm eq}$ (Menou 2012). In contrast, MHD simulations show flow reversal (i.e., eastward jets become westward) with increasing $T_{\rm eq}$ (Batygin et al. 2013; Heng & Workman 2014; Rogers & Komacek 2014). Bypassing the question of wind direction, in this work, we explore the mean equatorial wind velocity from energetic grounds using statistical evidence of the heating efficiency (Thorngren & Fortney 2018).

The remainder of the manuscript is organized as follows. In Sec. 2, we outline the HJ and OD model. We present the resulting circulation profiles in Sec. 3. We discuss our results and conclude in Sec. 4.

2. Theory

2.1. Conductivity Profile

The machinery of the OD mechanism is underlined by the fact that – owing to thermal ionization of alkali metals that are present in trace abundances – HJ atmospheres are rendered weakly conductive. Accordingly, the first step in our analysis is to delineate the conductivity profile. We divide the Hot Jupiter into radiative and convective layers, with the radiative-convective boundary (RCB) located at 100 bars.[2]

In practice, the functional form of the conductivity profile is only important in the vicinity of the RCB. In the radiative layer, we approximate the temperature as isothermal by averaging over the plane-parallel static grey atmosphere (Guillot 2010):

$$T^4 = \frac{3T_{\rm int}^4}{4}\left(\frac{2}{3}+\tau\right) + \frac{3T_{\rm eq}^4}{4}\left\{\frac{2}{3}+\frac{2}{3\zeta}\left[1+\left(\frac{\zeta\tau}{2}-1\right)e^{-\zeta\tau}\right] + \frac{2\zeta}{3}\left(1-\frac{\tau^2}{2}\right)E_2(\zeta\tau)\right\}, \tag{1}$$

where T is the temperature in the atmosphere, $T_{\rm int}$ the intrinsic temperature, $T_{\rm eq}$ the equilibrium temperature of the HJ, τ the optical depth, $\zeta := \frac{\kappa_{\rm v}}{\kappa_{\rm th}}$ the opacity ratio, and $E_n(z) := \int_1^\infty t^{-n}e^{-zt}{\rm d}t$ the exponential integral function. We adopt Guillot (2010) values for HD 209458 b's visible and thermal opacity: $\kappa_{\rm v} = 0.004\,{\rm cm^2\,g^{-1}}$ and $\kappa_{\rm th} = 0.01\,{\rm cm^2\,g^{-1}}$, respectively.

Below the RCB, we assume a polytropic relation $P \propto \rho^\gamma$, where P is the pressure and γ is the polytropic index. We obtain γ by fitting along an adiabat from the hydrogen-helium equation of state of Chabrier & Debras (2021). Because the conductivity rises rapidly in the interior, the contribution of the deep interior to the heating is small. Thus, our polytropic fit suffices for our purposes. To this end, we note that anomalous heating need not be deposited at the center of the convective envelope to sustain the planetary radius in an inflated state. That is to say, energy deposited sufficiently deep in the envelope, a radius that translates to a pressure-level on the order of 10 kbar (Batygin et al. 2011; Spiegel & Burrows 2013; Ginzburg & Sari 2016; Komacek & Youdin 2017, and the references therein), is sufficient. Re-inflating a HJ from a cold state, however, requires deeper heat deposition (e.g., Thorngren et al. 2021). Generally, concerns of Ohmic re-inflation of close-in giant planets (Hartman et al. 2016; Grunblatt et al. 2017) – while fascinating – are beyond the scope of this work.

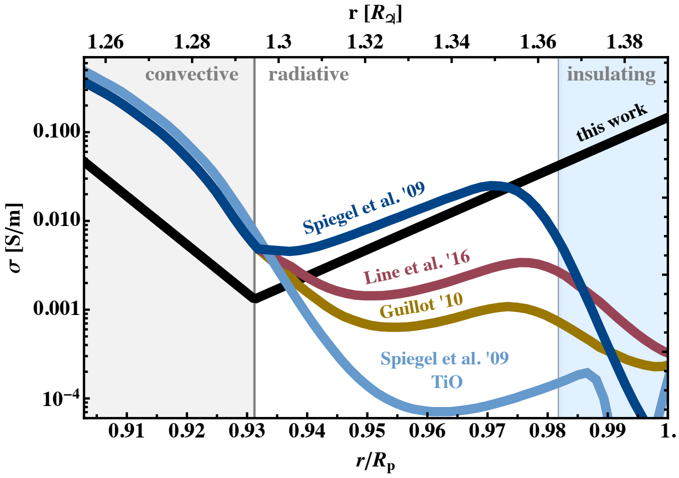

Fig. 1. Conductivity profile of this work (black) in comparison with Kumar et al. (2021) for HD 209458 b. The references above the lines indicate the atmosphere model used by Kumar et al. (2021) to compute the respective conductivity profile, namely: Guillot (2010), Line et al. (2016), and Spiegel et al. (2009) with and without TiO in the atmosphere.

The ionization fraction of alkali metals is determined by Saha's equation:

$$\frac{n_j^+ n_{\rm e}}{n_j - n_j^+} = \left(\frac{m_{\rm e}kT}{2\pi\hbar^2}\right)^{3/2}\exp\left(-\frac{I_j}{kT}\right), \tag{2}$$

where the subscript j denotes the respective alkali metal, n_j^+ its positively ionized number density, I_j its ionization potential, and n_j its total number density, k is the Boltzmann constant, $m_{\rm e}$ the electron mass, $n_{\rm e}$ the electron number density, and $\hbar$ the reduced Planck constant. We can solve this equation in the weakly-ionization limit ($n_j^+ \ll n_j$) to obtain the electron number density. Throughout this study, we use the proto-Solar abundances of Lodders (2003), $Z_\odot = 0.0149$, to obtain n_j.

Assuming a classical free electron gas, the conductivity σ in the isothermal layer simplifies to an exponential function (Batygin & Stevenson 2010):

$$\sigma(r) = \sigma_{\rm RCB}\exp\left(\frac{r - r_{\rm RCB}}{2H}\right), \tag{3}$$

where the subscript RCB denotes the respective quantity value at the RCB, r the radial distance, and H the pressure scale height.

The adiabatic conductivity expression is more complex. While a semi-analytic profile can in principle be readily derived, for simplicity, we approximate this layer with an exponential profile as well: $\sigma = \sigma_{\rm RCB}\exp\left[(r_{\rm RCB} - r)/H_{\rm fit}\right]$, where $H_{\rm fit}$ is the free parameter used to fit the profile to the adiabatic expression.

Recently, Kumar et al. (2021) undertook a sophisticated calculation of σ. We do not reproduce their treatment but compare their results with our simple estimate in Fig. 1. Crucially, all conductivity profiles show a drop close to $R \sim 1.365\,R_{♃} = 0.98\,R_{\rm p}$, and we model this with an insulating boundary condition at $r = R$.

2.2. Velocity Profile

Most HJs orbit their host star on circular orbits (Bonomo et al. 2017). Tidal despinning will lock those planets, creating a con-

[2] A more complete approach would solve the Schwarzschild criterion to obtain the RCB pressure. Because our results depend only weakly on the exact value, we approximate it by 100 bars for consistency with Batygin & Stevenson (2010). Recent statistical studies (Thorngren et al. 2019; Sarkis et al. 2021) arrive at considerably shallower RCB values, which expands our weather layer size slightly (see Appendix C).

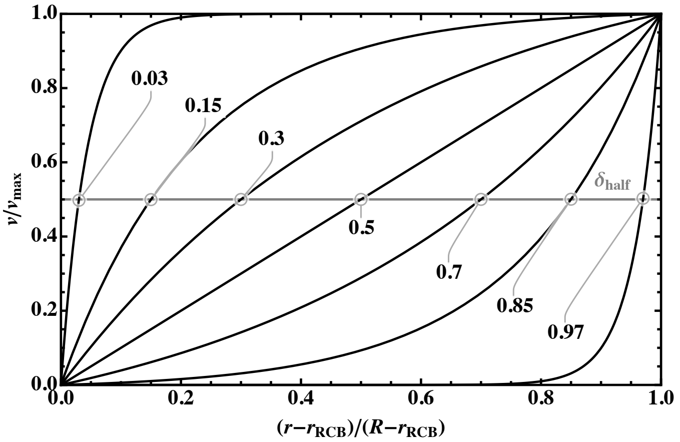

Fig. 2. Zonal wind velocity at the equator (Eq. 4) as a function of radius for five different relative half-velocity radii δ_{half}.

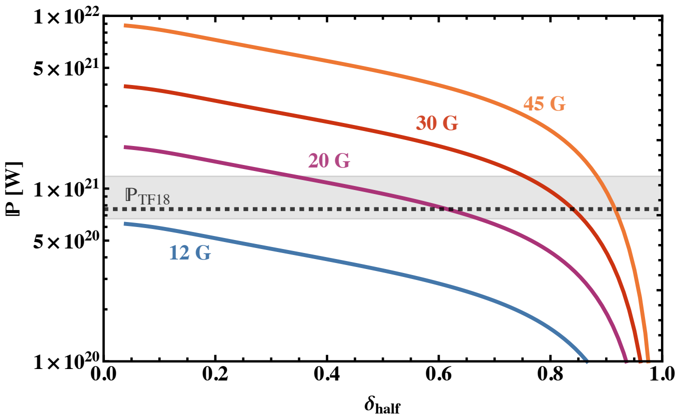

Fig. 3. OD rate as a function of the wind profile δ_{half} for HD 209458 b with $v_{max} = 2\,\mathrm{km\,s^{-1}}$ (Snellen et al. 2010). The colors represent different magnetic field strengths at the equator and the gray region indicates the anomalous heating rate computed by Thorngren & Fortney (2018).

stantly irradiated *dayside* and a *nightside* that faces away from the host star (Hut 1981). This unbalance in heating leads to a pressure gradient, which balances with the planet's rotation and drag to creates strong winds on HJs (for a review, see Showman et al. 2012). For HD 209458 b, for example, Snellen et al. (2010) observed wind velocities at around $(2 \pm 1)\,\mathrm{km\,s^{-1}}$ in the upper atmosphere.

Various GCMs (e.g., Heng et al. 2011; Parmentier et al. 2013; Showman et al. 2015; Menou 2019), analytical theory (e.g., Showman & Polvani 2010, 2011), and observations of hot-spot shifts (e.g., Knutson et al. 2007) indicate that these winds manifest as a single dominant eastward jet.

In presence of 10 – 100 G magnetic fields (Yadav & Thorngren 2017; Cauley et al. 2019), significant induction of electrical currents is unavoidable. While the conductivity of the atmosphere is insufficient for the resulting Lorentz force to fully suppress the circulation (Batygin et al. 2013), in the convective interior, conductivity rises rapidly ensuring the dominance of the magnetic drag (e.g., Liu et al. 2008; Rogers & Showman 2014). As a consequence, zonal winds will be dissipated completely at or below the RCB (velocity $\boldsymbol{v} = 0$ for $r \leq r_{RCB}$).

This leads us to parametrize the velocity field in the radiative layer by:

$$\boldsymbol{v}(r,\theta) = v_{max} \cdot \left(\frac{e^{\xi r} - e^{\xi r_{RCB}}}{e^{\xi R} - e^{\xi r_{RCB}}} \right) \sin\theta \cdot \hat{\phi}, \tag{4}$$

where v_{max} is the maximum velocity at the equator, R the OD radius, θ the polar angle, and $\hat{\phi}$ the basis vector in azimuthal direction. ξ is a free parameter of dimension 1/length that controls the radial form of the zonal jet by damping or enhancing the penetration depth. To simplify the comparison between various velocity profiles[3] and give a physical intuition, we introduce the (dimensionless) relative half-velocity radius δ_{half}, which is the relative distance between the RCB and the OD radius where v decreased by 1/2 (Fig. 2). If $\delta_{half} = 0.5$, the velocity decreases linearly towards the RCB. If $0.5 < \delta_{half} < 1$, the velocity drops off more quickly and the zonal jets are confined to a smaller region in the upper atmosphere. Lastly, if $0 < \delta_{half} < 0.5$, the velocity decreases more slowly and the zonal jet is more extended.

[3] In principle, a number of velocity profiles would fit our requirements. For example, the power law $\left(\frac{r-r_{RCB}}{R-r_{RCB}}\right)^{\xi}$ also works. However, the derivative of this profile diverges for $0 < \xi < 1$, introducing unnecessary complications into the analytical treatment.

2.3. Ohmic Dissipation Rate

Since the introduction of the OD model (Batygin & Stevenson 2010; Batygin et al. 2011), a number of authors have explored various dependencies of this heating mechanism (e.g., Wu & Lithwick 2012; Spiegel & Burrows 2013; Ginzburg & Sari 2016), and the basic theoretical framework of OD is well documented in the literature. Hence, we will skip the derivation here and only state the equations that we are solving.

To obtain the OD rate $\mathbb{P}$, we need to compute:

$$\mathbb{P} = \int \frac{\boldsymbol{j}_{ind}^2}{\sigma} \mathrm{d}V, \tag{5}$$

where $\mathrm{d}V$ is the volume element and $\boldsymbol{j}_{ind}$ is the induced current density. We can obtain $\boldsymbol{j}_{ind}$ from Ohm's law:

$$\boldsymbol{j}_{ind} = \sigma(\boldsymbol{v} \times \boldsymbol{B} - \nabla\Phi), \tag{6}$$

where $\boldsymbol{B}$ is the HJ's magnetic field, which we approximate by a dipole. Φ, the electric potential, is obtained by solving a variation of Poisson's equation that comes from continuity of the current density:

$$\nabla \cdot \sigma\nabla\Phi = \nabla \cdot \sigma\,(\boldsymbol{v} \times \boldsymbol{B})\,. \tag{7}$$

The radius of an inflated gas giant is predominately determined by its interior entropy (Zapolsky & Salpeter 1969). Heat deposited into the radiative layer radiates away before influencing the adiabat noticeably (Spiegel & Burrows 2013). Consequently, Eq. 5 is restricted to evaluation in the convective zone to determine the radius inflation.

3. Results

3.1. Weather Layer Depth

We computed $\mathbb{P}$ in the range of $0 < \delta_{half} < 1$, which represents both, shallow and deep zonal flows (Fig. 2). The zonal wind profile influences the OD rate by an order of magnitude (Fig. 3). This is expected since the volume that contributes to the generation of the induced current (Eq. 6) increases. More precisely: the OD rate scales roughly like the volume integral $\int \boldsymbol{v}\mathrm{d}V$.

In addition, the anomalous heating rates of Thorngren & Fortney (2018) are easily reproduced for magnetic fields stronger than $\sim 12\,\mathrm{G}$. Moreover, for HD 209458 b, we expect $\delta_{half} = 0.82$

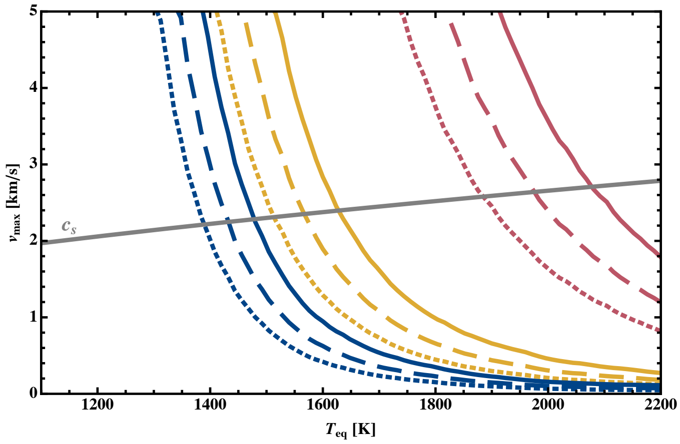

Fig. 4. Equatorial wind velocity v_{max} needed to reproduce the anomalous heating powers of Thorngren & Fortney (2018) as a function of equilibrium temperature. Blue represents $0.5\,M_{♃}$, yellow $1\,M_{♃}$, and red $3\,M_{♃}$. The dotted, dashed, and solid lines represent $\delta_{half} = 0.5/0.8/0.9$, respectively.

($\xi = 51\,R_{♃}^{-1}$, $P(\delta_{half}) = 0.34$ bar) for 27.72 G (scaling law from Yadav & Thorngren 2017) and $v_{max} = 2\,\mathrm{km\,s^{-1}}$ (Snellen et al. 2010). As $P \propto e^{-r/H}$, $v \propto e^{\xi r} \propto P^{-\xi H} \approx P^{-0.52}$, which falls more slowly than $v \propto P^{-5/2}$ found by Ginzburg & Sari (2016) and confines the circulation to the top 3% of the HJ. In other words, our results indicate that a shallow weather layer is sufficient to explain the radius anomaly.

3.2. Zonal Wind Velocities

In the last section, we derived the flow geometry (δ_{half}) given the equatorial wind velocity. Conversely, we can ask: What is the zonal wind velocity required, given a flow geometry, to inflate a HJ sufficiently?

For this, we probe three HJ masses – $0.5\,M_{♃}$, $1\,M_{♃}$, and $3\,M_{♃}$ – for three zonal flow configurations, respectively: a linear decrease ($\delta_{half} = 0.5$), a shallow weather layer similar to HD 209458 b ($\delta_{half} = 0.8$), and a very shallow weather layer ($\delta_{half} = 0.9$). The intrinsic temperature, HJ radius, and magnetic field strength are taken from the results of Thorngren & Fortney (2018) and Yadav & Thorngren (2017).

The resulting velocities decrease with equilibrium temperature like a power law (Fig. 4). This originates from a roughly linear increase in the anomalous heating power and the magnetic field with equilibrium temperature (i.e., $\mathbb{P} \propto T_{eq}$ and $B \propto T_{eq}$). Since $\mathbb{P} \propto v^2 B^2$, this leads to $v \propto \sqrt{\mathbb{P}}/B \propto T^{-1/2}$. The physical interpretation for this effect is the damping of zonal flows due to strong magnetic drag.

Once we reach higher equilibrium temperatures, however, the magnetic field strength stays roughly constant (Yadav & Thorngren 2017). Therefore, the velocity stays roughly constant as well. Furthermore, lower δ_{half} values (i.e., more extended zonal jets) lead to lower velocities, since OD is more efficient (see also discussion below).

On the lower end of the spectrum, the equilibrium temperatures are too low to ionize sufficient amounts of alkali metals and planetary magnetic fields are weak. Hence, the zonal winds flow with little resistance, but also deposit little power into the planet's interior. Ultimately, the velocities diverge, indicating that OD cannot inflate efficiently at low T_{eq} – an arguably trivial result. These extremely high velocities can be interpreted as upper bounds, which lose their physical meaning once the speed of sound is significantly exceeded and shock-induced dissipation sets in.

4. Discussion

In this work, we explored the physics of OD in HJs and derived an analytic expression for the power deposited into the convective interior as a function of wind penetration depth. This equation (see Eq. A.3) gives a simple and robust order-of-magnitude estimate.

We found that the wind profile has an order-of-magnitude influence on the power output. This effect must be taken into account in any detailed model of OD. Additionally, the scaling law allows to constrain unobservable planetary parameters from direct observations. If, for example, one would obtain the equatorial wind velocity of a HJ via spectroscopy, our scaling relation predicts the flow geometry with little effort.

In order to explain the radius anomaly, shallow weather layers appear sufficient. For HD 209458 b, we predict that the flow velocity drops by a factor of 2 at ~ 0.4 bar compared to the wind velocity at the photosphere. While this velocity slope is rather steep, the Richardson number still exceeds 0.25, indicating that the Kelvin-Helmholtz instability never sets in. The weather layer size is on the lower end of GCM simulations and on the higher end of MHD simulations (Sec. 1). This model does not apply to low equilibrium temperatures (~ 1000 K) though, where a radius excess above the jovian radius can be attributed to an extended radiative layer – without the need for an interior heating mechanism.

Lastly we found that, for a constant δ_{half}, the equatorial wind speed decreases with equilibrium temperature like a power law

$$v_{max}(T_{eq}) \propto (T_{eq} - T_0)^{-\alpha}, \ \alpha \approx 1/2, \tag{8}$$

where T_0 is a constant that evaluates to $T_0 \sim 1000\,\mathrm{K} - 1800\,\mathrm{K}$ depending on planet-specific parameters (radius, mass, etc.), before saturating at a few hundred meters per seconds. This profile shows a similar decrease to Menou (2012), Rogers & Komacek (2014) and Koll & Komacek (2018) at around $T_{eq} \approx 1500$ K (Fig. 5). In contrast though, Menou (2012) suggests more rapid velocity damping due to magnetic drag towards higher equilibrium temperatures. Moreover, Rogers & Komacek (2014) arrive at considerably lower wind velocities (and hence OD rates) due to their numerical treatment ($\sim 2 \times 10^{18}$ W for $B = 15$ G and $v = 160\,\mathrm{m\,s^{-1}}$ at depth). All of these models predict lower velocities than recently observed in ultra-hot Jupiters (e.g., $5.5\,\mathrm{km\,s^{-1}}$ for WASP-76 b, Seidel et al. 2021). In this vein, our model suggests that only a very shallow circulation layer is required to explain the radius inflation in such a system, although a massive high-metallicity core could undoubtably alter this assertion. More fundamentally, our model assumptions are rendered invalid in the ultra-hot Jupiter regime ($\gtrsim 2000$ K) where magnetic Reynolds numbers greatly exceed unity. Another distinction in atmospheric wind measurements between $T_{eq} < 2000$ K HJs and ultra hot Jupiters may lie in that the sampled pressure-levels of the atmosphere are vastly different. Ultimately, a more detailed analysis of MHD effects (e.g., Rogers 2017; Hindle et al. 2019; Beltz et al. 2021) is required to understand their extremely fast wind velocities.

While recent theoretical evidence points towards enhanced bulk metallicities of HJs (e.g., Thorngren et al. 2016; Müller et al. 2020; Schneider & Bitsch 2021, see also Appendix B), those effects are subdominant to the uncertainty in the magnetic

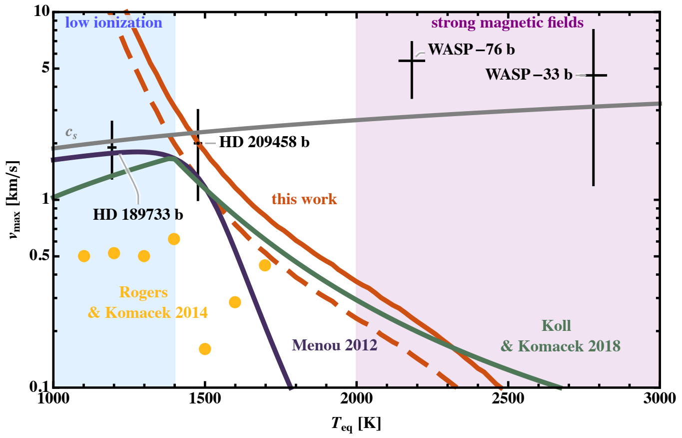

Fig. 5. Zonal wind velocity as a function of equilibrium temperature for various models. Menou (2012) (purple) and this work's solid line (red) compute the velocity at the equator, whereas Rogers & Komacek (2014) (yellow), Koll & Komacek (2018) (green), and this work's dashed line (red) compute the mean zonal flow. The planetary parameters of HD 209458 b and a magnetic field of $B = 15$ G were hold constant throughout our simulation. The velocity measurements are taken from Snellen et al. (2010) (HD 209458 b), Louden & Wheatley (2015) (HD 189733 b), Seidel et al. (2021) (WASP-76 b), and Cauley et al. (2021) (WASP-33 b).

field and the velocity ($\mathbb{P} \propto \sqrt{Z}v^2B^2$). Nonetheless, since OD exclusively predicts a correlation between alkali metal abundance and radius inflation, atmospheric enrichment in alkali metals, as observed by (Welbanks et al. 2019), might be an important contributing factor for this mechanism. For this study though, as we do not claim to predict the exact anomalous heating power for *a specific planet* but rather introduce a general and robust extension to the Ohmic heating paradigm, they are of little concern for the validity of our results.

As the atmospheric composition, the wind velocity, and dipole field strength of HJs are currently poorly constrained, we emphasize that this study can only yield an estimate of the broad circulation profile, rather than a precise prediction.[4] Likewise, more observational data of wind velocities in HJs, especially in the $T_{eq} \sim 1500$ K range, would aid in constraining δ_{half} empirically. Lastly, Ohmic dissipation in the ultra-hot Jupiter regime remains poorly understood. Future studies could build upon recent analytical (Hindle et al. 2019, 2021) or numerical (Beltz et al. 2021) work to account for those objects self-consistently. Nonetheless, this work shows that OD can not only explain the radius inflation problem, but also allows us to peak deep into HJ atmospheres, and thereby, give us new insights into their remarkable structure.

Acknowledgements. B.B., acknowledges the support of the European Research Council (ERC Starting Grant 757448-PAMDORA). K.B. is grateful to Caltech, and the David and Lucile Packard Foundation for their generous support.

References

Arras, P. & Socrates, A. 2010, The Astrophysical Journal, 714, 1
Atreya, S. K., Crida, A., Guillot, T., et al. 2016, eprint arXiv:1606.04510
Batygin, K., Stanley, S., & Stevenson, D. J. 2013 [1307.8038]
Batygin, K. & Stevenson, D. J. 2010 [1002.3650]
Batygin, K., Stevenson, D. J., & Bodenheimer, P. H. 2011 [1101.3800]

[4] Temperature inversion in the atmosphere (i.e., in the presence of TiO) already alters the conductivity (and hence the OD rate) by two orders of magnitude.

Beltz, H., Rauscher, E., Roman, M., & Guilliat, A. 2021, Exploring the Effects of Active Magnetic Drag in a GCM of the Ultra-Hot Jupiter WASP-76b
Bodenheimer, P., Laughlin, G., & Lin, D. N. C. 2003, The Astrophysical Journal, 592, 555
Bodenheimer, P., Lin, D. N. C., & Mardling, R. A. 2001, The Astrophysical Journal, 548, 466
Bonomo, A. S., Desidera, S., Benatti, S., et al. 2017, Astronomy & Astrophysics, 602, A107
Burrows, A., Sudarsky, D., & Lunine, J. 2003, Astrophys.J., 596, 587
Cauley, P. W., Shkolnik, E. L., Llama, J., & Lanza, A. F. 2019, Nature Astronomy, 3, 1128
Cauley, P. W., Wang, J., Shkolnik, E. L., et al. 2021, The Astronomical Journal, 161, 152
Chabrier, G. & Debras, F. 2021, The Astrophysical Journal, 917, 4
Charbonneau, D., Brown, T. M., Latham, D. W., & Mayor, M. 2000, The Astrophysical Journal, 529, L45
Ginzburg, S. & Sari, R. 2016, The Astrophysical Journal, 819, 116
Grunblatt, S. K., Huber, D., Gaidos, E., et al. 2017, The Astronomical Journal, 154, 254
Guillot, T. 2010 [1006.4702]
Hartman, J. D., Bakos, G. Á., Bhatti, W., et al. 2016, The Astronomical Journal, 152, 182
Heng, K., Menou, K., & Phillipps, P. J. 2011, Monthly Notices of the Royal Astronomical Society, 413, 2380
Heng, K. & Workman, J. 2014, The Astrophysical Journal Supplement Series, 213, 27
Henry, G. W., Marcy, G. W., Butler, R. P., & Vogt, S. S. 2000, The Astrophysical Journal, 529, L41
Hindle, A. W., Bushby, P. J., & Rogers, T. M. 2019, The Astrophysical Journal Letters (2019), Volume 872, Number 2 [1902.09683]
Hindle, A. W., Bushby, P. J., & Rogers, T. M. 2021, The Astrophysical Journal, 922, 176
Hut, P. 1981, A&A, 99, 126
Knutson, H. A., Charbonneau, D., Allen, L. E., et al. 2007, Nature, 447, 183
Koll, D. D. B. & Komacek, T. D. 2018, The Astrophysical Journal, 853, 133
Komacek, T. D. & Youdin, A. N. 2017, 844, 94
Kumar, S., Poser, A. J., Schöttler, M., et al. 2021, Physical Review E, 103
Laughlin, G., Crismani, M., & Adams, F. C. 2011, The Astrophysical Journal, 729, L7
Li, C., Ingersoll, A., Bolton, S., et al. 2020, 4, 609
Line, M. R., Stevenson, K. B., Bean, J., et al. 2016, The Astronomical Journal, 152, 203
Liu, J., Goldreich, P., & Stevenson, D. 2008, 196, 653
Lodders, K. 2003, Astrophys. J., 591, 1220
Louden, T. & Wheatley, P. J. 2015, The Astrophysical Journal, 814, L24
Menou, K. 2012, ApJ, 745, 138
Menou, K. 2019, Monthly Notices of the Royal Astronomical Society: Letters, 485, L98
Menou, K. 2020, Monthly Notices of the Royal Astronomical Society, 493, 5038
Müller, S., Ben-Yami, M., & Helled, R. 2020, 903, 147
Parmentier, V., Showman, A. P., & Lian, Y. 2013, Astronomy & Astrophysics, 558, A91
Rauscher, E. & Menou, K. 2013, The Astrophysical Journal, 764, 103
Rogers, T. M. 2017, Nature Astronomy, 1
Rogers, T. M. & Komacek, T. D. 2014, The Astrophysical Journal, 794, 132
Rogers, T. M. & Showman, A. P. 2014, The Astrophysical Journal, 782, L4
Sarkis, P., Mordasini, C., Henning, T., Marleau, G. D., & Mollière, P. 2021, Astronomy and Astrophysics, 645, A79
Schneider, A. D. & Bitsch, B. 2021, 654, A71
Seidel, J. V., Ehrenreich, D., Allart, A., et al. 2021 [2107.09530]
Showman, A. P., Fortney, J. J., Lewis, N. K., & Shabram, M. 2012, The Astrophysical Journal, 762, 24
Showman, A. P., Lewis, N. K., & Fortney, J. J. 2015, The Astrophysical Journal, 801, 95
Showman, A. P. & Polvani, L. M. 2010, Geophysical Research Letters, 37, n/a
Showman, A. P. & Polvani, L. M. 2011, The Astrophysical Journal, 738, 71
Snellen, I. A. G., de Kok, R. J., de Mooij, E. J. W., & Albrecht, S. 2010, Nature, 465, 1049
Spiegel, D. S. & Burrows, A. 2013, The Astrophysical Journal, 772, 76
Spiegel, D. S., Silverio, K., & Burrows, A. 2009, Astrophys.J., 699, 1487
Stassun, K. G., Collins, K. A., & Gaudi, B. S. 2017, The Astronomical Journal, 153, 136
Stevenson, D. 1982, Planetary and Space Science, 30, 755
Thorngren, D. P. & Fortney, J. J. 2018, The Astronomical Journal, 155, 214
Thorngren, D. P., Fortney, J. J., Lopez, E. D., Berger, T. A., & Huber, D. 2021, The Astrophysical Journal Letters, 909, L16
Thorngren, D. P., Fortney, J. J., Murray-Clay, R. A., & Lopez, E. D. 2016, 831, 64
Thorngren, D. P., Gao, P., & Fortney, J. J. 2019 [1907.07777]
Tremblin, P., Chabrier, G., Mayne, N. J., et al. 2017, The Astrophysical Journal, 841, 30
Welbanks, L., Madhusudhan, N., Allard, N. F., et al. 2019, The Astrophysical Journal Letters, 887, L20
Wu, Y. & Lithwick, Y. 2012, The Astrophysical Journal, 763, 13
Yadav, R. K. & Thorngren, D. P. 2017, ApJ, 849, L12
Youdin, A. N. & Mitchell, J. L. 2010, The Astrophysical Journal, 721, 1113
Zapolsky, H. S. & Salpeter, E. E. 1969, The Astrophysical Journal, 158, 809

Appendix A: Solving the Electric Potential Equation

The conductivity profile in this work is given by

$$\sigma(r) = \begin{cases} \sigma_{\mathrm{RCB}} \exp\left(\frac{r-r_{\mathrm{RCB}}}{2H}\right) & \text{for } r_{\mathrm{RCB}} < r \leq R \\ \sigma_{\mathrm{RCB}} \exp\left(\frac{r_{\mathrm{RCB}}-r}{H_{\mathrm{fit}}}\right) & \text{for } r_{\max} < r \leq r_{\mathrm{RCB}} \\ \sigma_{\max} & \text{for } r \leq r_{\max} \end{cases}, \tag{A.1}$$

where $r_{\max}$ is the radius at which the conductivity reaches the maximum value of $\sigma_{\max} = 1 \times 10^6\,\mathrm{S\,m^{-1}}$. Accordingly, we solve Eq. 7 in those three regions, assuming a dipole magnetic field

$$\boldsymbol{B} = \nabla \times k_m \left(\frac{\sin\theta}{r^2}\right)\hat{\phi}, \tag{A.2}$$

where k_m is the dipole magnetic moment.

This is done by decomposing the equation into spherical harmonics $Y_l^m(\theta, \phi)$, which yields that only the $l = 2$ and $m = 0$ component contribute to the Ohmic dissipation rate. We obtain the constants of integration by enforcing continuity, assuming that the electric potential is zero at the center, $\Phi(r = 0) = 0$, and that there is an insulating boundary layer at R: $\boldsymbol{j}_{\mathrm{ind}}(R, \theta, \phi) \cdot \hat{r} = 0$. Typical values for R include the transit radius of the planet or the radius at which the conductivity in the radiative layer drops significantly. The resulting induced current density is evaluated as described in Sec. 2.3. The Ohmic dissipation rate becomes

$$\mathbb{P} = v_{\max}^2 B^2 \sigma_{\mathrm{RCB}} \cdot f(r_{\mathrm{RCB}}, R, R_{\mathrm{p}}, H, H_{\mathrm{fit}}, \xi), \tag{A.3}$$

where f is given by:

$$\begin{aligned}
&- 64\pi H^2 H_{\mathrm{fit}} R_{\mathrm{p}}^6 \left(4H_{\mathrm{fit}} - r_{\mathrm{RCB}}\right)\left(-6H_{\mathrm{fit}} r_{\mathrm{RCB}} + 12H_{\mathrm{fit}}^2 + r_{\mathrm{RCB}}^2\right) \\
&\cdot \Bigg(\xi^2(2H\xi + 1)(6H\xi + 1) r_{\mathrm{RCB}}^3 \Bigg(e^{\frac{R}{2H}}\left(48H^2 - 12HR + R^2\right)\left(\mathrm{Ei}\left(\xi R\right) - \mathrm{Ei}\left(\xi r_{\mathrm{RCB}}\right)\right) \\
&- \left(48H^2 + 12HR + R^2\right)\left(\mathrm{Ei}\left(\xi R + \frac{R}{2H}\right) - \mathrm{Ei}\left(\xi r_{\mathrm{RCB}} + \frac{r_{\mathrm{RCB}}}{2H}\right)\right)\Bigg) \\
&+ r_{\mathrm{RCB}}^3\left(-e^{\frac{R}{2H}+\xi R}\right)\left(\xi\left(-24H^2\xi(12H\xi + 5) + 6H\xi R + R\right) - 1\right) \\
&+ e^{\xi r_{\mathrm{RCB}}}\Bigg(e^{\frac{R}{2H}}\left(24H^2\xi\left(48H^2 - 12HR + R^2\right) + \xi(2H\xi + 1)(6H\xi + 1) r_{\mathrm{RCB}}^2\left(48H^2 - 12HR + R^2\right)\right. \\
&\left. + 4H\xi(3H\xi + 2) r_{\mathrm{RCB}}\left(48H^2 - 12HR + R^2\right) - r_{\mathrm{RCB}}^3\right) \\
&- 2H\xi\left(48H^2 + 12HR + R^2\right) e^{\frac{r_{\mathrm{RCB}}}{2H}}\left(6H\left(\xi r_{\mathrm{RCB}}\left(\xi r_{\mathrm{RCB}} + 1\right) + 2\right) + r_{\mathrm{RCB}}\left(\xi r_{\mathrm{RCB}} - 2\right)\right)\Bigg)\Bigg)^2 \\
&/\Bigg\{5 r_{\mathrm{RCB}}^3\left(e^{\xi R} - e^{\xi r_{\mathrm{RCB}}}\right)^2\Bigg(\left(48H^2 + 12HR + R^2\right) e^{\frac{r_{\mathrm{RCB}}}{2H}} \\
&\cdot \left(288H^2 H_{\mathrm{fit}}\left(H_{\mathrm{fit}} + 2H\right) - 6\left(H_{\mathrm{fit}} + 2H\right) r_{\mathrm{RCB}}^3 + 12\left(H_{\mathrm{fit}} + 2H\right)\left(H_{\mathrm{fit}} + 3H\right) r_{\mathrm{RCB}}^2 - 96H\left(H_{\mathrm{fit}} + H\right)\left(H_{\mathrm{fit}} + 2H\right) r_{\mathrm{RCB}} + r_{\mathrm{RCB}}^4\right) \\
&- 12H\left(H_{\mathrm{fit}} + 2H\right) e^{\frac{R}{2H}}\left(48H^2 - 12HR + R^2\right)\left(4H_{\mathrm{fit}} r_{\mathrm{RCB}} + 24HH_{\mathrm{fit}} - 8H r_{\mathrm{RCB}} - r_{\mathrm{RCB}}^2\right)\Bigg)^2\Bigg\}
\end{aligned} \tag{A.4}$$

with $\mathrm{Ei}(z) := -\int_{-z}^{\infty} e^{-t}/t\,\mathrm{d}t$.

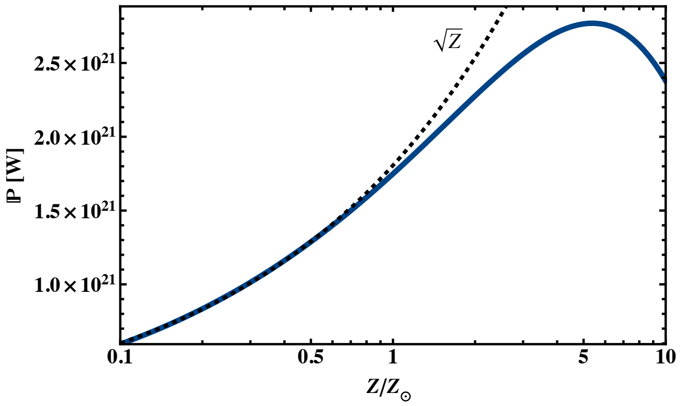

Fig. B.1. Ohmic dissipation rate as a function of metallicity assuming the parameters of HD 209458 b and a linearly decreasing jet (δ_{half} = 0.5).

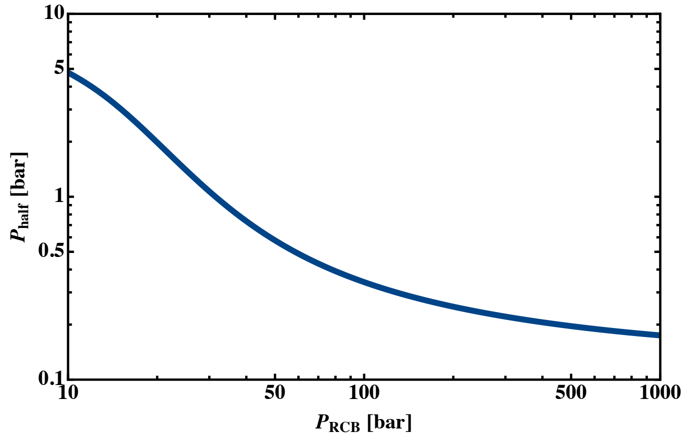

Fig. C.1. Half velocity pressure P_{half} as a function of RCB pressure P_{RCB} assuming the parameters of HD 209458 b.

Appendix B: Influence of Metallicities

The solar system's giant planets are enhanced in metals compared to solar values (e.g., Atreya et al. 2016; Li et al. 2020). While it is not yet clear how planets form, interior modeling (e.g., Thorngren et al. 2016; Müller et al. 2020) and planet formation models (e.g., Schneider & Bitsch 2021) suggest that similarly enhanced metallicities are plausible for HJs.

The influence of metals on the OD rate is a tradeoff between increased electric conductivity and atmospheric contraction due to higher mean molecular weight. For small metallicities, the increase in conductivity dominates, leading to $\mathbb{P} \propto \sqrt{Z}$. Increasing the metallicity further, contraction starts to play a significant role, damping the dissipation rate (Fig. B.1). Nonetheless, the change of $\mathbb{P}$ is clearly subdominant to the uncertainty in velocity and magnetic field strength.

Appendix C: Shallow RCB Layers

As mentioned in Sec. 2, the depth of the RCB differs significantly between studies using the Schwarzschild criterion (e.g., Burrows et al. 2003; Batygin et al. 2011; Kumar et al. 2021) and recent statistically motivated studies (Thorngren et al. 2019; Sarkis et al. 2021). The latter arrive at considerably shallower RCB depths, which may be a consequence of depositing the entire heat in the center of the planet. In fact, Youdin & Mitchell (2010) argue that turbulent diffusion in the radiative layer pushes the RCB down to the kbar range. In any case, the penetration depth depends only weakly on the exact value (Fig. C.1). Hence, we conclude that our results are robust against variations in the RCB depth.